Monte Carlo simulation of a mixed spin 2 and spin $\frac{1}{2}$ Ising ferrimagnetic system

Monte Carlo simulation of a mixed spin 2 and spin $\frac{1}{2}$ Ising ferrimagnetic system

G M Buendía† and J A Liendo‡

† Departamento de Física, Universidad Simón Bolívar, Apartado 89000, Caracas 1080, Venezuela
‡ Centro de Física, Instituto Venezolano de Investigaciones Científicas, Apartado 21827, Caracas 1020, Venezuela

Abstract. The critical behaviour of a mixed ferrimagnetic Ising system on a square lattice in which the two interpenetrating square sublattices have spins σ $(\pm\frac{1}{2})$ and S $(\pm 2, \pm 1, 0)$ has been studied. We carried out exact ground state calculations and performed Monte Carlo simulations to obtain the finite-temperature phase diagram of the model. We found that the system that includes only a nearest-neighbour interaction and the crystal field does not have a compensation point. Also, our study seems to indicate that, contrary to effective-field predictions, there is no tricritical point at nonzero temperature for this model; however a more elaborate analysis will be needed to draw a definite conclusion on this point.

1. Introduction

Intensive experimental work is currently being carried out to synthesize stable, crystalline materials with spontaneous magnetic moments at room temperature [1]. Ferrimagnetic ordering seems to play a crucial role in these materials and the study of ferrimagnetism has rapidly become a very active field of research. In a ferrimagnetic material, the existence of a compensation temperature, i.e. a temperature below the critical temperature, T_c, at which the resultant magnetization vanishes [2], is an interesting possibility with important technological applications. This behaviour is possible due to the different temperature dependences of the sublattice magnetizations.

An important number of ferrimagnetic materials with very promising characteristics are currently being synthesized. New bimetallic linear chains have been produced and characterized by the use of the so called 'brick and mortar' technique [3]. Also, two mixed-metal ferrimagnetic assemblies of the type $\{NBu_4[MFe(ox)_3]\}_x$, with M = Ni, Fe and NBu_4 = tetra(n-butyl)ammonium ion, have been obtained using a trisoxalatoferrate, [Fe(ox)$_3$], as the building block. Magnetization measurements revealed magnetic phase transitions at $T_c = 28$ (43) K for M = Ni (Fe) which are appreciably higher than those associated with the corresponding ferromagnets, $\{NBu_4[NiCr(ox)_3]\}_x$, $T_c = 14$ K, and $\{NBu_4[FeCr(ox)_3]\}_x$, $T_c = 12$ K [4].

Although most currently used magnetic materials are inorganic and based on metallic or ionic lattices, new classes of magnets have recently been obtained with molecular organic chemistry techniques. Ferrimagnetic materials referred to as Prussian blue analogues, with a critical temperature of 240 K, have been reported [5]. The recently synthesized amorphous $V(TCNE)_x.y$ (solvent), where TCNE is tetracyanoethylene, orders ferrimagnetically above 400 K [6]. Another experimental group has just announced the synthesis of compounds such

as $N(n\text{-}C_nH_{2n+1})_4Fe^{II}Fe^{III}(C_2O_4)_3$ with $n = 3$–5 that have critical temperatures between 35 and 48 K. Some of these compounds have compensation temperatures near 30 K [7]. Major breakthroughs are expected in the field of molecular magnetism. Organic materials with properties such as solubility in organic solvents, biocompatibility, transparency and easy processing and fine-tuning of their magnetic properties are not far from reality.

The remarkable experimental progress achieved to date in the synthesis of ferrimagnetic materials requires a deeper understanding of the theoretical characterization of these materials. Mixed Ising systems provide simple but interesting models to study ferrimagnetic ordering. Several techniques, such as high-temperature series expansion [8], renormalization group [9], mean-field [10], effective-field [11, 12] and nonperturbative approaches [13, 14], have been used to investigate the magnetic properties of these systems. There is also a solution of a mixed Ising system on a Union Jack lattice on a two-dimensional manifold in the parameter space [15]. Mean- and effective-field theories predict the existence of tricritical [10, 12] and compensation points [10, 11] in mixed Ising systems described by Hamiltonians which only include nearest-neighbour and crystal field interactions. However, recent studies based on nonperturbative methods such as Monte Carlo and numerical transfer matrix methods [14] indicate that the predictions given by mean- and effective-field theories are not reliable for these models.

In this article, we present a Monte Carlo study of a mixed spin Ising system, where the spins σ, that take two possible values, $\pm\frac{1}{2}$, and the spins S, that take five possible values, ± 2, ± 1, 0, are nearest neighbours and interact antiferromagnetically, while spins of the same type are next-nearest neighbours. Ground state diagrams are calculated exactly and Monte Carlo simulations are carried out to obtain the finite-temperature phase diagram and to explore the existence of a compensation point. Effective-field theory predicts that this system has a tricritical point at a nonzero temperature, but gives no prediction about the existence of a compensation point [12].

2. The model and its ground states

We study a 2D Ising model with spins, $S = \pm 2$, ± 1, 0 and $\sigma = \pm 1/2$, located in alternating sites of a square lattice, such that the S and the σ spins are nearest neighbours and the next-nearest neighbours are always spins of the same type. A Hamiltonian for this model that includes only nearest-neighbour and external field interactions is

$$H = -J_1 \sum_{\langle nn \rangle} S_i \sigma_j - J_2 \sum_{\langle nn \rangle} S_i^2 \sigma_j - H_{1/2} \sum_j \sigma_j - H_1 \sum_i S_i + D \sum_i S_i^2 \quad (1)$$

where J_1 and J_2 are the exchange interaction parameters, $H_{1/2}$ and H_1 are external fields and D is the crystal field, all in energy units. The parameter J_1 is chosen to be negative such that the coupling between nearest neighbours is antiferromagnetic.

In order to generate the ground state diagrams, we have calculated the energy of each configuration of a 2×2 unit cell [16]. Taking into account rotational symmetry, there are 45 such configurations with different degrees of degeneracy. Table 1 shows the energies and degeneracies of the 45 configurations. The ground state of the model depends on the values of the parameters in the Hamiltonian. For example, in figure 1 we show the ground state diagram for the J_1–J_2–D model (for which all the parameters in the Hamiltonian are zero, except J_1, J_2 and D). The boundaries between the regions are obtained by pairwise equating the ground state energies.

To compare our results with those predicted by effective-field theory [12], we restrict our Monte Carlo simulations to the J_1–D (J_2, $H_{1/2}$ and H_1 are all zero) model. The ground state

Table 1. Ground state configurations, degeneracies and energies for the 2×2 unitary spin cells. The symbol convention is as follows: $\sigma = \frac{1}{2}$, +; $\sigma = -\frac{1}{2}$, −; $S = 0$, 0; $S = +1$, ↑; $S = -1$, ↓; $S = 2$, ⇑; $S = -2$, ⇓.

No	Configuration		Degeneracy	Energy per site
1	0	+	1	$E_1 = \frac{1}{4} H_{1/2}$
	+	0		
2	0	+	2	$E_2 = -J_1 - 2J_2 - \frac{1}{4} H_{1/2} - \frac{1}{2} H_1 + D$
	+	⇑		
3	0	+	2	$E_3 = -\frac{1}{2} J_1 - \frac{1}{2} J_2 - \frac{1}{4} H_{1/2} - \frac{1}{4} H_1 + \frac{1}{4} D$
	+	↑		
4	0	+	2	$E_4 = \frac{1}{2} J_1 - \frac{1}{2} J_2 - \frac{1}{4} H_{1/2} + \frac{1}{4} H_1 + \frac{1}{4} D$
	+	↓		
5	0	+	2	$E_5 = J_1 - 2J - 2 - \frac{1}{4} H_{1/2} + \frac{1}{2} H_1 + D$
	+	⇓		
6	↑	+	2	$E_6 = -\frac{3}{2} J - 1 - \frac{5}{2} J_2 - \frac{1}{4} H_{1/2} - \frac{3}{4} H_1 + \frac{5}{4} D$
	+	⇑		
7	⇑	+	2	$E_7 = -\frac{1}{2} J_1 - \frac{5}{2} J_2 - \frac{1}{4} H_{1/2} - \frac{1}{4} H_1 + \frac{5}{4} D$
	+	↓		
8	⇑	+	2	$E_8 = -4J_2 - \frac{1}{4} H_{1/2} + 2D$
	+	⇓		
9	↑	+	1	$E_9 = -J_1 - J_2 - \frac{1}{4} H_{1/2} - \frac{1}{2} H_1 + \frac{1}{2} D$
	+	↑		
10	↑	+	2	$E_{10} = -J_2 - \frac{1}{4} H_{1/2} + \frac{1}{2} D$
	+	↓		
11	↑	+	2	$E_{11} = \frac{1}{2} J_1 - \frac{5}{2} J_2 - \frac{1}{4} H_{1/2} + \frac{1}{4} H_1 + \frac{5}{4} D$
	+	⇓		
12	↓	+	1	$E_{12} = J_1 - J_2 - \frac{1}{4} H_{1/2} + \frac{1}{2} H_1 + \frac{1}{2} D$
	+	↓		
13	↓	+	2	$E_{13} = \frac{3}{2} J_1 - \frac{5}{2} J_2 - \frac{1}{4} H_{1/2} + \frac{3}{4} H_1 + \frac{5}{4} D$
	+	⇓		
14	⇓	+	1	$E_{14} = 2J_1 - 4J_2 - \frac{1}{4} H_{1/2} + H_1 + 2D$
	+	⇓		
15	⇑	+	1	$E_{15} = -2J_1 - 4J_2 - \frac{1}{4} H_{1/2} - H_1 + 2D$
	+	⇑		
16	0	−	1	$E_{16} = \frac{1}{4} H_{1/2}$
	−	0		
17	0	−	2	$E_{17} = J_1 + 2J_2 + \frac{1}{4} H_{1/2} - \frac{1}{2} H_1 + D$
	−	⇑		
18	0	−	2	$E_{18} = \frac{1}{2} J_1 + \frac{1}{2} J_2 + \frac{1}{4} H_{1/2} - \frac{1}{4} H_1 + \frac{1}{4} D$
	−	↑		
19	0	−	2	$E_{19} = -\frac{1}{2} J_1 + \frac{1}{2} J_2 + \frac{1}{4} H_{1/2} + \frac{1}{4} H_1 + \frac{1}{4} D$
	−	↓		
20	0	−	2	$E_{20} = -J_1 + 2J_2 + \frac{1}{4} H_{1/2} + \frac{1}{2} H_1 + D$
	−	⇓		
21	⇑	−	1	$E_{21} = 2J_1 + 4J_2 + \frac{1}{4} H_{1/2} - H_1 + 2D$
	−	⇑		
22	⇑	−	2	$E_{22} = \frac{3}{2} J_1 + \frac{5}{2} J_2 + \frac{1}{4} H_{1/2} - \frac{3}{4} H_1 + \frac{5}{4} D$
	−	↑		
23	⇑	−	2	$E_{23} = \frac{1}{2} J_1 + \frac{5}{2} J_2 + \frac{1}{4} H_{1/2} - \frac{1}{4} H_1 + \frac{5}{4} D$
	−	↓		
24	⇑	−	2	$E_{24} = 4J_2 + \frac{1}{4} H_{1/2} + 2D$
	−	⇓		
25	↑	−	1	$E_{25} = J_1 + J_2 + \frac{1}{4} H_{1/2} - \frac{1}{2} H_1 + \frac{1}{2} D$
	−	↑		

Table 1. (Continued)

No	Configuration			Degeneracy	Energy per site
26	↑	−		2	$E_{26} = J_2 + \frac{1}{4}H_{1/2} + \frac{1}{2}D$
	−	↓			
27	↑	−		2	$E_{27} = -\frac{1}{2}J_1 + \frac{5}{2}J_2 + \frac{1}{4}H_{1/2} + \frac{1}{4}H_1 + \frac{5}{4}D$
	−	⇓			
28	↓	−		1	$E_{28} = -J_1 + J_2 + \frac{1}{4}H_{1/2} + \frac{1}{2}H_1 + \frac{1}{2}D$
	−	↓			
29	↓	−		2	$E_{29} = -\frac{3}{2}J_1 + \frac{5}{2}J_2 + \frac{1}{4}H_{1/2} + \frac{3}{4}H_1 + \frac{5}{4}D$
	−	⇓			
30	⇓	−		1	$E_{30} = -2J_1 + 4J_2 + \frac{1}{4}H_{1/2} + H_1 + 2D$
	−	⇓			
31	0	−		2	$E_{31} = 0$
	+	0			
32	0	−		4	$E_{32} = -\frac{1}{2}H_1 + D$
	+	⇑			
33	0	−		4	$E_{33} = -\frac{1}{4}H_1 + \frac{1}{4}D$
	+	↑			
34	0	−		4	$E_{34} = \frac{1}{4}H_1 + \frac{1}{4}D$
	+	↓			
35	0	−		4	$E_{35} = \frac{1}{2}H_1 + D$
	+	⇓			
36	⇑	−		2	$E_{36} = -H_1 + 2D$
	+	⇑			
37	⇑	−		4	$E_{37} = -\frac{3}{4}H_1 + \frac{5}{4}D$
	+	↑			
38	⇑	−		4	$E_{38} = -\frac{1}{4}H_1 + \frac{5}{4}D$
	+	↓			
39	⇑	−		4	$E_{39} = 2D$
	+	⇓			
40	↑	−		2	$E_{40} = -\frac{1}{2}H_1 + \frac{1}{2}D$
	+	↑			
41	↑	−		4	$E_{41} = \frac{1}{2}D$
	+	↓			
42	↑	−		4	$E_{42} = \frac{1}{4}H_1 + \frac{5}{4}D$
	+	⇓			
43	↓	−		2	$E_{43} = \frac{1}{2}H_1 + \frac{1}{2}D$
	+	↓			
44	↓	−		4	$E_{44} = \frac{3}{4}H_1 + \frac{5}{4}D$
	+	⇓			
45	⇓	−		2	$E_{45} = H_1 + 2D$
	+	⇓			

diagram for this system is given by the line $J_2 = 0$ in figure 1. The ordered phases of the J_1–D model at $T = 0$ are separated at the two critical values corresponding to $D/|J_1| = \frac{2}{3}$ (between the ground state of the $S = \pm 2$, $\sigma = \pm\frac{1}{2}$ model and that of the $S = \pm 1$, $\sigma = \pm\frac{1}{2}$ model) and $D/|J_1| = 2$ (between the ground state of the $S = \pm 1$, $\sigma = \pm\frac{1}{2}$ model and that of the $S = 0$, $\sigma = \pm\frac{1}{2}$ model).
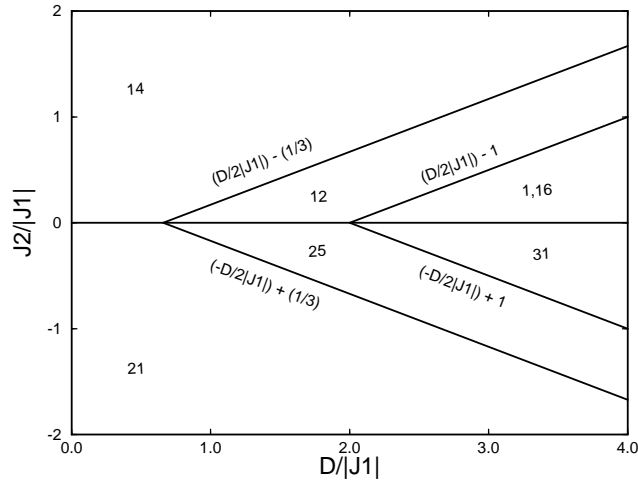
Figure 1. The ground state diagram for the J_1–J_2–D model. The configurations of the unit cell in each of the five regions are labelled as in table 1.

3. The Monte Carlo simulation

We use standard Monte Carlo techniques [17] to simulate the Hamiltonian described by (1) on square lattices of $L \times L$ sites with periodic boundary conditions. Configurations are generated by sweeping through the lattice and flipping the spins one at a time. The flips are accepted or rejected by the heat bath algorithm, such that, once the equilibrium has been reached, the probability of a particular configuration is proportional to the Boltzmann factor. We choose $L = 60$. Data were generated with 10^5 Monte Carlo steps per site after discarding the firsts 10^3 steps per site. The error bars were calculated by taking all the measurements and grouping them in ten blocks. The values obtained in this way are statistically independent and we can take their standard deviation as the error estimate.

We calculated the internal energy per site,

$$E = (1/L^2)\langle H \rangle \tag{2}$$

the specific heat,

$$C = (\beta^2/L^2)[\langle H^2 \rangle - \langle H \rangle^2] \tag{3}$$

the sublattice magnetizations, M_1 and M_2, defined as

$$M_1 = \frac{2}{L^2}\left\langle \sum_i S_i \right\rangle \tag{4}$$

and

$$M_2 = \frac{2}{L^2}\left\langle \sum_j \sigma_j \right\rangle \tag{5}$$

the total magnetization per spin, $M = (M_1 + M_2)/2$, and the order parameters

$$O_\pm = \frac{1}{L^2}\left\langle \left| \sum_{i,j}(S_i \pm \sigma_j) \right| \right\rangle. \tag{6}$$

The averages are taken over all the configurations, the sums over i are over all the sites with S spins and the sums over j are over all the sites with σ spins. Each sum has $L^2/2$

terms. In order to verify our results, we compared them with exact enumeration studies for $L = 2$. We also checked that the ground state diagrams are reproduced for different combinations of parameters in the Hamiltonian.

The compensation point, T_{comp}, can be located by finding the crossing point between the absolute values of the sublattice magnetizations,

$$|M_1(T_{comp})| = |M_2(T_{comp})| \tag{7}$$

with the conditions

$$\text{sign}[M_1(T_{comp})] = -\text{sign}[M_2(T_{comp})] \text{ and } T_{comp} < T_c. \tag{8}$$

These conditions ensure that at T_{comp} the two sublattice magnetizations cancel each other, whereas at the critical temperature, T_c, both go to zero.
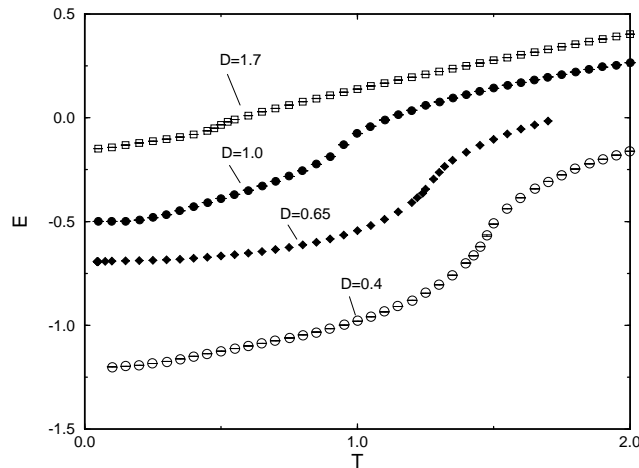

Figure 2. Energy against T for several values of $D/|J_1|$, $J_1 = -1$, in the different regions shown in figure 1 corresponding to $J_2 = 0$. In most cases the error bars cannot be observed because they are smaller than the symbols chosen.

4. Results

We start by testing the predictions for the critical temperatures of the J_1–D model given by the effective-field theory [12]. The ground state for this system corresponds to the line $J_2 = 0$ in figure 1. By means of a Monte Carlo simulation we explore the finite-temperature behaviour of the magnetization, the energy, the specific heat and the order parameter in the different regions of the parameter space. All the calculations were performed with $J_1 = -1$.

In figure 2, we show the energy as a function of the temperature for several values of $D/|J_1|$. As expected, the ground state energies coincide with those calculated in table 1. Several specific heat curves are shown in figure 3; the critical temperatures (T_c) are obtained by locating the maxima of the curves. In figure 4, we show the finite-temperature phase diagram calculated with the Monte Carlo method. Also, in the same figure, we present the results given by effective-field theory [12]. Notice that the two curves have a similar shape but effective-field theory overestimates the critical temperatures. In the limit, $D \to -\infty$, the Monte Carlo results are in excellent agreement with those of a nearest-neighbour spin $\frac{1}{2}$ Ising model, $T_c(\text{exact}) = 2.269$. Effective-field theory predicts the existence of a tricritical point
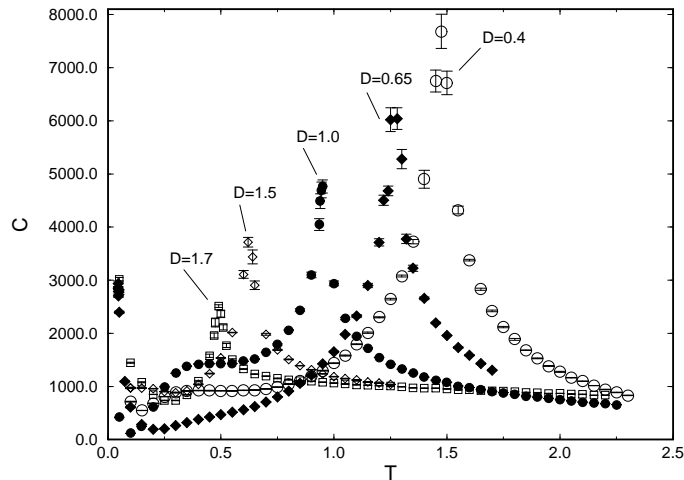
Figure 3. Specific heat against T for different values of $D/|J_1|$, $J_1 = -1$. The location of the maximum gives an estimate of T_c.
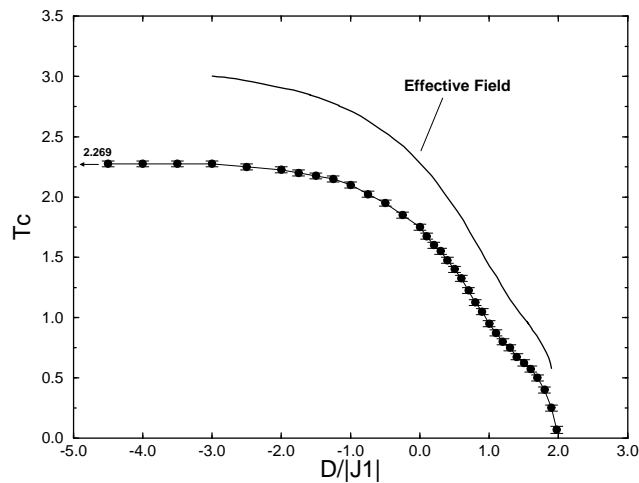

Figure 4. The finite-temperature phase diagram for the J_1–D model. Monte Carlo results are indicated by solid circles with error estimates. The solid line corresponds to the effective-field approximation [12]. In the limit $D \to -\infty$ the system reduces to a nearest-neighbour spin $\frac{1}{2}$ Ising system. The Monte Carlo simulations give the correct value of T_c in this limit, $T_c(\text{exact}) = 2.269$.

at $D/|J_1| = 1.965$, $T_c = 0.5138$ [12]. Our small-scale simulations show no evidence of a tricritical point at finite temperature, instead our results suggest that the critical temperature goes to zero when $D/|J_1|$ goes to the critical value of two.

In figure 5, we show the total magnetization, $(M_1 + M_2)/2$, as a function of the temperature, for several values of the parameter $D/|J_1|$. To avoid confusion due to the well known phenomenon of the flipping of the entire spin system near the critical point, we choose the convention $M_1 > 0$ and $M_2 < 0$, such that when flipping is observed at high temperatures we change the signs of the magnetizations to adhere to the convention.

The magnetization curves do not seem to indicate the presence of a nonzero tricritical temperature near the value $D/|J_1| = 2$.

It is interesting to notice, in figure 5, the peculiar behaviour of the magnetization near the critical values of $D/|J_1|$ shown in figure 1 ($D/|J_1| = \frac{2}{3}$, 2). When $D/|J_1|$ is very small the magnetization behaves as that of a ferromagnet, decaying from its maximum value at $T = 0$ following a Q type curve in the Néel classification [2], but as $D/|J_1|$ increases and approaches its critical value of $\frac{2}{3}$, the magnetization at low temperature presents a rather rapid decrease from its value at $T = 0$, as shown in figure 5(a) for $D = 0.65$. This low-temperature behaviour is not predicted by Néel theory of ferrimagnetism. A similar behaviour has been observed in amorphous ferrites [18].

When $D/|J_1| = \frac{2}{3}$, the zero-temperature value of the magnetization is 0.5, which indicates that the ground state is a mixed state where the S spins are distributed in the $S = 2$ or $S = 1$ state with equal probability, and the σ spins take the value of $-\frac{1}{2}$. When $D/|J_1|$ is very close to and greater than $\frac{2}{3}$ (the next region in the ground state diagram) the total magnetization at low temperature increases very rapidly from its zero-temperature value before decaying at T_c (M type behaviour), but as $D/|J_1|$ keeps increasing the rise of the low-temperature magnetization value is less pronounced, until, for a $D/|J_1|$ value near unity, the magnetization behaves again in the standard way for a ferromagnet, decreasing from its zero-temperature value in a Q type curve. As the next critical point, $D/|J_1| = 2$, is approached, the rapid drop in the total magnetization at low temperatures is observed again, but in this case is due to the fact that the critical temperature is very low.

The magnetization curves indicate that this model has no compensation point, i.e. the total magnetization is never zero below T_c (behaviour type N). It is evident that the conditions given by (7) and (8) are not satisfied. The absolute values of the sublattice magnetizations are equal only at T_c, where both go to zero. Also, we observe that the S sublattice is the one with the strongest dependence on the $D/|J_1|$ parameter.

5. Conclusions

We have applied a Monte Carlo algorithm to the study of a mixed Ising model on a square lattice, where spins $S = \pm 2, \pm 1, 0$ are alternated with spins $\sigma = \pm \frac{1}{2}$. Choosing antiferromagnetic nearest-neighbour interactions provides us with a simple but interesting model of ferrimagnetic behaviour.

We have calculated exactly the ground state energies for a Hamiltonian with nearest-neighbour interactions, external fields and the crystal field, and have shown the phase diagram for a particular combination of parameters in the Hamiltonian.

In order to perform the Monte Carlo simulation and compare our results with those obtained by effective-field theory, we chose to keep only the parameters associated with the first-order interaction and the crystal field: J_1 and D respectively. We presented results for the magnetization, the energies and the specific heat for this model, as functions of the temperature.

We found no evidence to support the effective-field prediction that the J_1–D model has a tricritical point at a nonzero temperature [12]. This discordance is not surprising since recent results for a similar model ($S = \pm 1, 0, \sigma = \pm \frac{1}{2}$), obtained with Monte Carlo and transfer matrix techniques, indicate that mean- and effective-field predictions for tricritical and compensation points are not reliable for these mixed systems [14]. However, a more detailed analysis with larger lattices, either by studying the behaviour of the eigenvalues of the transfer matrix [19] or by calculating the critical exponents, will be necessary to
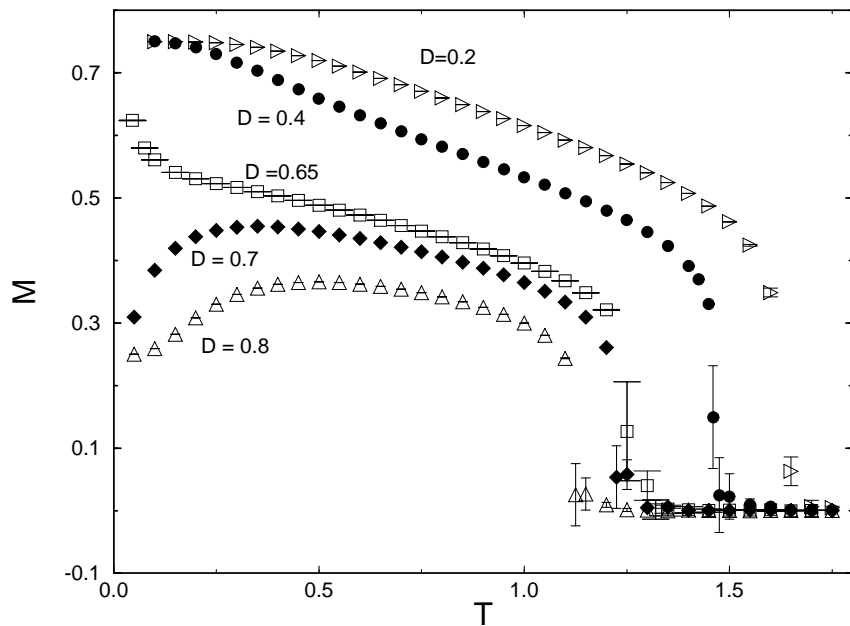
(a)
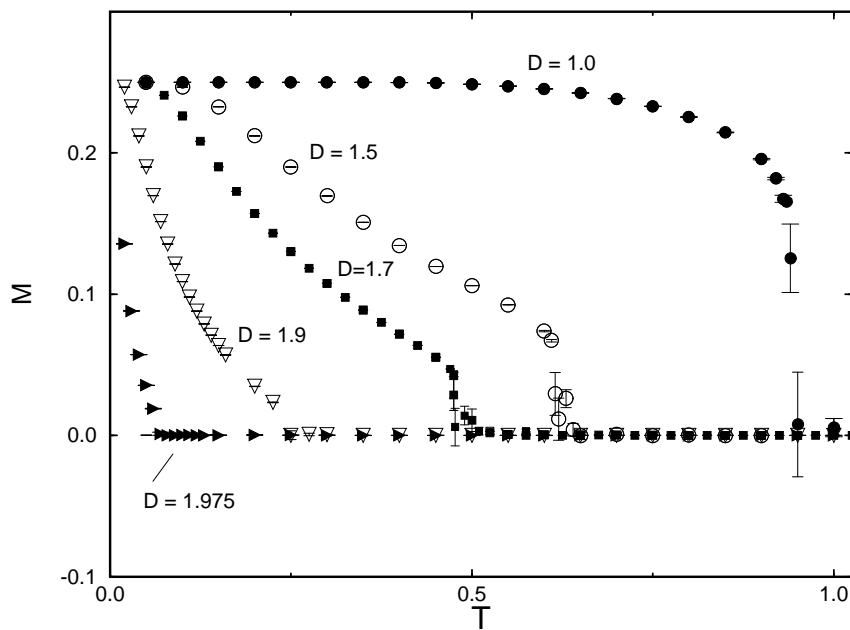
(b)

Figure 5. The total magnetization $M = (M_1 + M_2)/2$ as a function of the temperature is shown in the different regions corresponding to $J_2 = 0$ in figure 1, $J_1 = -1$. Notice how T_c shifts toward zero as $D/|J_1|$ increases towards the critical value of two. (a) Total magnetization against T for $D = 0.2$, 0.4, 0.65, 0.7 and 0.8. (b) Total magnetization against T for $D/|J_1| = 1$, 1.5, 1.7, 1.9 and 1.975.

establish a definite conclusion on the existence of a tricritical point.

Also, we found that there is no compensation point for the J_1–D model. A previous work carried out on the $S = \pm 1, 0, \sigma = \pm \frac{1}{2}$ model indicates that the next-nearest interactions between the σ type spins are responsible for the existence of compensation points [14], and a recent work shows that this is also the case for the present model [20].

This system has a more complex phase diagram than the spin 1–spin $\frac{1}{2}$ system. Its ground state diagram presents two critical values $(D/|J_1| = \frac{2}{3}, 2)$ whereas the spin 1–spin $\frac{1}{2}$ model has only one $(D/|J_1| = 2)$. This complexity is evident in the low-temperature behaviour of the total magnetization, that shows a strong dependence on the $D/|J_1|$ parameter. It is interesting to notice that when $D/|J_1|$ approaches from below the critical value of $\frac{2}{3}$, the total magnetization curve has a peculiar shape characterized, at low temperatures, by a very rapid drop from its zero-temperature value, followed by a somewhat more standard ferromagnetic type decay (Q type material) as the temperature increases. This behaviour is not described by the Néel theory of ferrimagnetism; however a similar behaviour has been reported in amorphous ferrites [18].

References

[1] Iwamura H and Miller J S (eds) 1993 *Proc. Conf. on Ferromagnetic and High Spin Molecular-Based Materials; Mol. Cryst. Liq. Cryst.* **232**
   Gatteshi D, Kahn O, Miller J S and Palacio F (eds) 1991 *Magnetic Molecular Materials (NATO ASI Series)* (Dordrecht: Kluwer)
[2] Néel L 1948 *Ann. de Phys.* **3** 137
[3] Willet R D, Wang Z, Molnar S, Brewer K, Landee C P, Turnbull M M and Zhang W 1993 *Mol. Cryst. Liq. Cryst.* **233** 277
[4] Okawa H, Matsumoto N, Tamaki H and Ohba M 1993 *Mol. Cryst. Liq. Cryst.* **233** 257
[5] Mallah T, Tiebaut S, Verdaguer M and Veillet P 1993 *Science* **262** 1554
[6] Manriquez J, Lee G T, Scott R, Epstein A and Miller J 1991 *Science* **252** 1415
[7] Mathonière C, Nuttall C J, Carlin S G and Day P 1996 *Inorg. Chem.* **35** 1201
[8] Hunter G J A, Jenkins R C L and Tinsley C J 1990 *J. Phys. A: Math. Gen.* **23** 4547
   Bowers R G and Yousif B Y 1983 *Phys. Lett.* **96A** 49
[9] Schofield S L and Bowers R G 1980 *J. Phys. A: Math. Gen.* **13** 3697
[10] Kaneyoshi T and Jascur M 1993 *J. Magn. Magn. Mater.* **118** 17
[11] Kaneyoshi T 1989 *Solid State Commun.* **70** 975
[12] Kaneyoshi T 1994 *Physica* A **205** 677
[13] Gonçalves L L 1985 *Phys. Scr.* **32** 248
   Iwashita T and Uryû N 1984 *J. Phys. Soc. Japan* **53** 721
[14] Buendía G M, Novotny M A and Zhang J 1994 *Computer Simulations in Condensed Matter Physics VII* ed D P Landau, K K Mon and H B Schüttler (Berlin: Springer) p 223
   Buendía G M and Novotny M A 1997 *J. Phys.: Condens. Matter* accepted for publication
[15] Lipowski A and Horiguchi T 1995 *J. Phys. A: Math. Gen.* **29** L261
[16] Karl G 1973 *Phys. Rev.* B **7** 2050
[17] Binder K 1979 *Monte Carlo Methods in Statistical Physics* ed K Binder (Berlin: Springer)
[18] Sugimoto M and Hiratsuka N 1982 *Japan. J. Appl. Phys.* **21** 197
   Srinivasan G, Uma Maheshwar Rao B, Zhao J and Seehra M S 1991 *Appl. Phys. Lett.* **58** 372
[19] Bartelt N C, Einstein T L and Roelofs L D 1986 *Phys. Rev.* B **34** 1616
[20] Buendía G M and Novotny M A 1997 *J. Physique* at press